Analysis of Diagnostic Capabilities for Degradation of Brushless Direct Current Motors Depending on Varying Simulation Data

Max Weigert[1]

[1]*Institute of Flight Systems and Automatic Control, Technical University of Darmstadt, Darmstadt , 64287, Germany*
weigert@fsr.tu-darmstadt.de

ABSTRACT

As the use of unmanned aerial vehicles (UAVs) becomes more widespread and their missions more complex, the need for safety measures for their technical components is also increasing. Among the components that are critical for the operation of UAVs, Brushless Direct Current (BLDC) motors are particularly important. This is due to their compact design and low number of wear parts, which make them well-suited for use in UAVs.

In this work, test rig and simulation data of BLDC motors degradation are utilized to investigate the capabilities and limitations of different machine learning algorithms. For this purpose, suitable features representing the motor behavior are discussed. Classification and regression models are applied to analyze both the fault type and the degradation progress. The simulated data allows for an assessment of the influence of noise and degradation progress on the diagnosis performance. Furthermore, characteristics of various fault types and the representation of their degradation process in the simulation are discussed. The database and the derived features are shared publicly under https://tudatalib.ulb.tu-darmstadt.de/handle/tudatalib/3912.

1. INTRODUCTION

The reliability of Brushless Direct Current (BLDC) motors is critical for the safe operation of unmanned aerial vehicles (UAVs), but designing effective condition monitoring approaches for these motors can be challenging due to a lack of operational data and uncertainty about the influence of noise and sample rate on diagnosis. Therefore, in this paper, the impact of noise and sample rate on the effectiveness of different machine learning algorithms for BLDC motor condition monitoring is analyzed using a simulation environment.

As discussed previously in (Weigert 2022) common degradation effects of BLDC motors can be reproduced simulatively based on conducted test bench experiments. Similar approaches have already been taken by (Wolfram et al. 2018), (Siddiolo and Buderath 2018) and (Gupta et al. 2021). Wolfram et al. (2018) utilized a test rig, which was further developed to parametrize the current BLDC motor simulation experimentally, in order to analyze and simulate an UAVs electrical powertrain and introduce several fault types to it. Siddiolo and Buderath (2018) generated experimental and synthetic Run-to-Failure datasets of an aeronautic fan on which they applied a Gaussian Process for health estimation. In (Gupta et al. 2021) the effects of high resistance contacts on BLDC motors are analyzed experimentally and in simulation. An overview on failure types of BLDC motors is given in (Kudelina et al. 2020), they identify mechanical, electrical and magnetic degradation to be the main failure classes of BLDC motors, which are represented in this work as well.

In (Shifat and Hur 2020) the influence of short circuits on BLDC motors is analyzed and a databased Remaining Useful Lifetime estimation is conducted. They show, that the Fast Fourier Transformation (FFT) can be applied to distinguish healthy and faulty BLDC operations. Statistical features that can be derived based on rotating machinery data in the time and frequency domain are discussed by (Lei et al. 2007) and appear to be a good basis for a condition monitoring system.

The approach of combining simulation and test bench results offers several advantages. Firstly, it reduces the material and time required to build up a sufficient database for condition monitoring with experimental data. Secondly, simulations can be used to derive tolerable noise levels and sample rates and their influence on fault classification. This is particularly useful when designing condition monitoring approaches before collecting operational data, as it allows for a more accurate prediction of the system's behavior under various conditions and an analysis of the required data quality for useful results. An analysis into the effects of noise on classification for different classifiers on several benchmark datasets has already been conducted by Hasan and Chu (2022). In (Bertolino et al. 2023) a PHM approach for Electromechanical Actuators is tested with simulated degradation patterns to estimate its future performance.

This work does also aim at comparing several algorithms on their condition monitoring performance. An overview on algorithmic approaches towards condition monitoring for rolling element bearings is given in (AlShorman et al. 2020). A comparison of several algorithmic approaches on motor current signal based health analysis is conducted in (Jiang et al. 2020), where the best results are received with Support Vector Machines.

2. METHODOLOGY

2.1. Variations in the simulation

In order to compare the impact of variations in noise, sample rate and degradation progress in the simulation on the condition monitoring, simulated datasets are derived at various stages of those parameters. Each simulated dataset consists of 11 operation scenarios, one of them being a healthy operation and 10 depicting distinguished degradation mechanisms. In each operation scenario, 12 motor examples with slight variations in their defining parameters are generated and simulated at 11 degradation progress levels. This allows for a total of 1452 operation points in each simulated dataset with labels for the degradation type and degradation progress.

Noise is introduced to the simulation as band-limited white noise passed through a low pass filter and added to ambient temperature and the supply voltage as those parameters are expected to be subject to slight fluctuations in reality as well. Simulation sets are derived for five noise levels of each parameter with each noise level a power of two larger than the previous level. With medium noise, the voltage range is 14.8 ± 0.2V and the temperature range is 20 ± 0.5°C. The sample rate is kept constant for all simulations but from each simulated dataset, 5 feature sets are derived with obtained measurement values at five different sample rates with one magnitude difference each. To analyze the influence of the degradation progress level, subsets of the data can be formed containing only early or late progress levels respectively.

The ambient temperature affects the simulation in two ways. Firstly, the airscrew torque relies on the derived air density. Secondly, the heat transfer from the system to its surroundings is modeled, determining the motor temperature. The motor temperature, in turn, has a linear impact on the winding resistance and is taken into account in the motor control.

2.2. Feature engineering

At each operation point a short timeseries with the same rotational speed setpoint for the motor controller is simulated. As the motor controller shall also prevent overheating, the achieved rotational speeds might differ between operational points even if the setpoint might still be reached within the performance limits of the simulated motor. The simulation contains a startup and a continuous operation phase with the temperature resistance in the startup phase temporarily lowered to reach an equilibrium prior to the continuous phase. Features are then derived based on the final section of the continuous phase.

For the measured timeseries of the three phase currents, the rotational speed and the duty cycle applied by the motor controller a set of features is calculated to describe each operational point. Most of those features are obtained by applying simple statistic measures to the data, which are listed in table 1. These are fully applied to the time domain and the root mean square, skewness, kurtosis and shape factor also to the frequency domain as a result of a FFT of the timeseries.

Table 1. Utilized statistical features.

measure	formula
mean	$\bar{x} = \frac{1}{n}\left(\sum_{i=1}^{n} x_i\right)$
standard deviation	$s = \sqrt{\frac{1}{n-1}\sum_{i=1}^{n}(x_i - \bar{x})^2}$
mean root square	$mrs = \left(\frac{1}{n}\left(\sum_{i=1}^{n}\sqrt{\lvert x_i\rvert}\right)\right)^2$
root mean square	$rms = \sqrt{\frac{1}{n}\left(\sum_{i=1}^{n} x_i^2\right)}$
mid	$mid = \frac{x_{max} - x_{min}}{2}$
skewness	$skewness = \frac{\frac{1}{n}\sum_{i=1}^{n}(x_i - \bar{x})^3}{\left(\frac{1}{n-1}\sum_{i=1}^{n}(x_i - \bar{x})^2\right)^{\frac{3}{2}}}$
kurtosis	$kurtosis = \frac{\frac{1}{n}\sum_{i=1}^{n}(x_i - \bar{x})^4}{\left(\frac{1}{n}\sum_{i=1}^{n}(x_i - \bar{x})^2\right)^2} - 3$
crest factor	$\frac{\lvert x\rvert_{max}}{rms}$
clearance factor	$\frac{\lvert x\rvert_{max}}{mrs}$
shape factor	$\frac{n * rms}{\sum_{i=1}^{n}\lvert x_i\rvert}$
impulse factor	$\frac{n * \lvert x\rvert_{max}}{\sum_{i=1}^{n}\lvert x_i\rvert}$

Additionally, the phase currents are subdivided into six sections, which are part of one electrical rotation, and the mean value and standard deviation in each position is

calculated as additional feature. This can only be done, if the sample rate is high enough to obtain at least one measured value per position. The sections are assigned based on the maxima positions of a smoothed current signal and a correlation of the expected and actual current. Further derived features from the FFT are the number of peaks above a prominence threshold relative to the maximum amplitude, the variance of those peaks and the frequencies and amplitudes of the five most prominent peaks.

2.3. Analyzed algorithms and optimization

The simulated data sets are kept rather small, with the main aim of facilitating the analysis of the performance of several algorithms, but also with the application-based aim of obtaining traceable results and identifying meaningful indicators of degradation. Therefore the focus is on tree based methods, namely Decision Trees (DT), Random Forests (RF) and eXtreme Gradient Boosting (XGB), and Support Vector Machines (SVM). Those models are implemented using the Scikit-Learn (Pedregosa et al. 2012) and the XGBoost (Chen and Guestrin 2016) library in python.

For the analyzed algorithms, two hyperparameter optimization steps are taken for each investigated simulation variation. First, a dataset with all calculated features is used to find an algorithmic setup, which does perform promisingly. Afterwards, the features are sorted based on their contribution to the algorithm obtained in the first optimization. A second optimization is done, in which the number of selected features is optimized as well. In this optimization, a small punishment for large algorithm structures and high numbers of features is included in the optimization objective to encourage lean models. The parameters themselves are kept rather small as well for the same reason. The parameter ranges for the different algorithms are listed in table 2. The bold parameter for each algorithm indicates the complexity parameter, which should be reduced in the second optimization step.

Table 2. Hyperparameter ranges for optimization.

	DT	**RF**	**XGB**		**SVM**
classification criterion	gini, entropy or log loss		merror	**C**	**1e-6 - 75**
regression criterion	squared error, friedman mse, absolute error or poisson		squared error	**kernel**	linear, poly, rbf, sigmoid
max depth	**3 - 35**	3 - 15	3 - 20	**degree**	1-5
min samples leaf	2 - 20		-	**gamma**	1e-6 - 10
max features	5 - 150		-	**coef0**	0 - 5
n estimators	-	**5 - 15**		**epsilon (regression)**	1e-6 - 10
learning rate	-		1e-3 - 0.5		
gamma	-		0-3		

The hyperparameter optimization is done in form of a Bayesian search applying the optuna library in python (Akiba et al. 2019). This shall enable quickly identifying promising hyperparameter combinations. To account for the random element in the search, each hyperparameter optimization has been repeated and the best result chosen.

The performance is evaluated with a four fold cross validation. Within the cross validation, the 12 simulated motor examples per operational state are each split into four groups, containing all measurements corresponding to three motor examples for each operational state respectively. For classification, the classification accuracy over all 11 operation classes is evaluated, for regression the root mean squared error.

3. DATA UNDERSTANDING

3.1. Sensor characteristics

Since the rotational speed is the controlled variable and the duty cycle is the manipulated variable, these only change marginally during the test depending on fluctuations over the revolution. The phase current, on the other hand, depends on the position of the motor and has a characteristic behavior in which it passes through six sections during one revolution, two with positive current, one with suppressed current, two with negative current and a second with suppressed current. This is depicted in figure 1 for four sample rate levels.

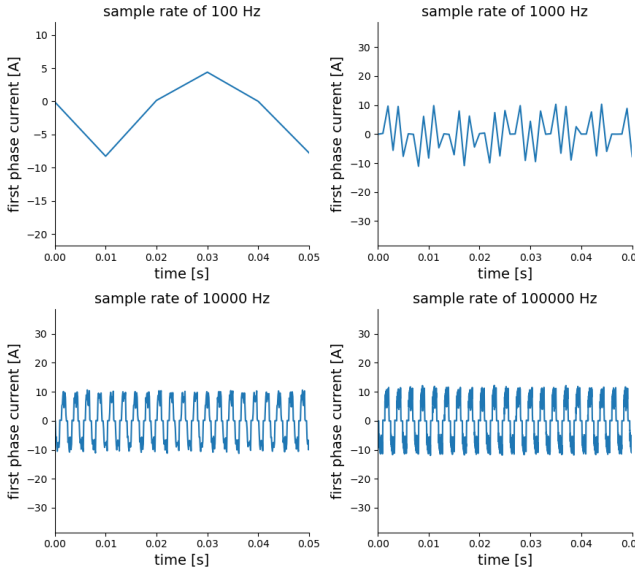

Figure 1. Phase current values at varying sample rates.

With a high sample rate, the pulse width modulation control is visible, as the simulated current alternates between values due to high frequent switching according to the duty cycle. With a medium sample rate, the alternating signal can't be resolved anymore and resembles noise. At lower frequencies, not all sections of a revolution are measured and the representation of the motor behavior loses considerable expressiveness. The highest sample rate of 1e6 Hz is not

depicted as it is barely distinguishable from sample rate 1e5 upon visual inspection.

3.2. Fault types

The simulated degradation mechanisms can be divided into three classes, electrical, mechanical and magnetic degradation. Electrical degradation is either represented by increased resistance or by short circuits between or within phases, mechanical degradation by increased local or overall friction values and magnetic degradation by reduced magnetic field strength. Those degradation patterns do impact the motor in distinguishable ways, which are further discussed in (Weigert 2022). In figure 2, the classes of a simulation dataset with minimal noise levels and highest sample rate are depicted. The figure axis of the mid current value of the most prominent current phase and the maximum amplitude of the duty cycle FFT are chosen based on a Principle Component Analysis to whose first two component those are the highest contributors. The axis are adjusted to contain a ratio of 10 between the smallest distance of datapoints along the axis and the medium distance of datapoints along the axis. This is due to the most interesting datapoints being those representing early degradation stages, which are close to each other and move further apart for increased degradation. This is depicted by an increasing transparency of the datapoints with increasing degradation.

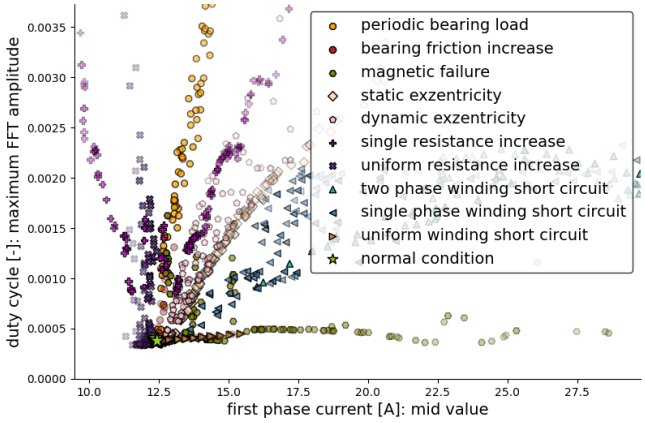

Figure 2. Simulation dataset features for high data quality.

The time behavior of the degradation mechanisms can follow separate patterns, as most of them are expected to accumulate over the number of revelations unrestrictedly while the short circuit degradation is depicted by an infinite short circuit resistance in nominal state, that approaches zero asymptotically with increasing number of revolutions. In figure 3 the root mean square value of the highest phase current for one motors magnetic degradation is depicted exemplarily for the first type of degradation time behavior. It is linear up to a motor specific threshold randomly chosen out of a specified revelation number band with a gradient chosen out of a specified gradient band as well. From then on, it resembles an exponential increase, which adopts the gradient at the transition point. This shall resemble experimental degradation patterns which could for example be observed in the FEMTO bearing dataset of the IEEE PHM challenge 2012 (Nectoux et al. 2012). The short-circuit resistance development over the number of revelations follows the formula given in Eq. 1 resulting in an hyperbola with the y and x axis as asymptotes.

$$R_s = \frac{R_{phase}}{(t+1) * f_{krit}} \tag{1}$$

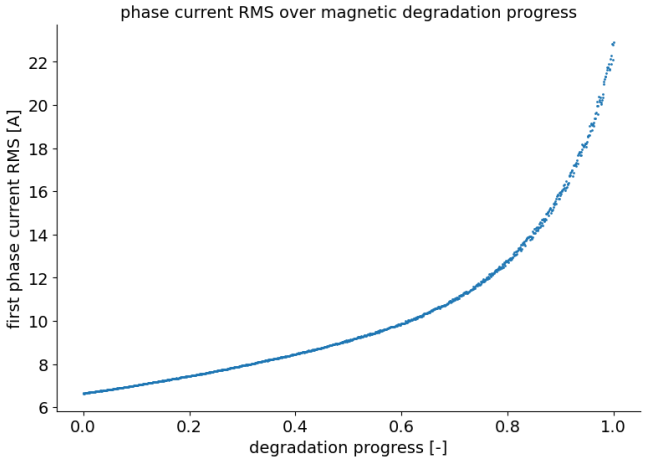

Figure 3. Magnetic motor degradation progress example.

3.3. Influence of noise and sample rate

The influence of the sample rate and simulation noise on the generated features is visualized in figure 4. Within the figure the already described features from figure 2, the mid current value of the most prominent current phase and the maximum amplitude of the duty cycle FFT, are plotted for varying noise and sample rate levels of the simulation dataset. To simplify the illustration, each depicted set has the same voltage and temperature noise. To enhance the influence analysis, in Table 3 and 4 the mean variances of the first two principle components within each dataset are listed. Two values are calculated, one being the variance of the mean values of each class and one being the mean value of the variance of each class, both are calculated as ratio to the overall variance of the dataset.

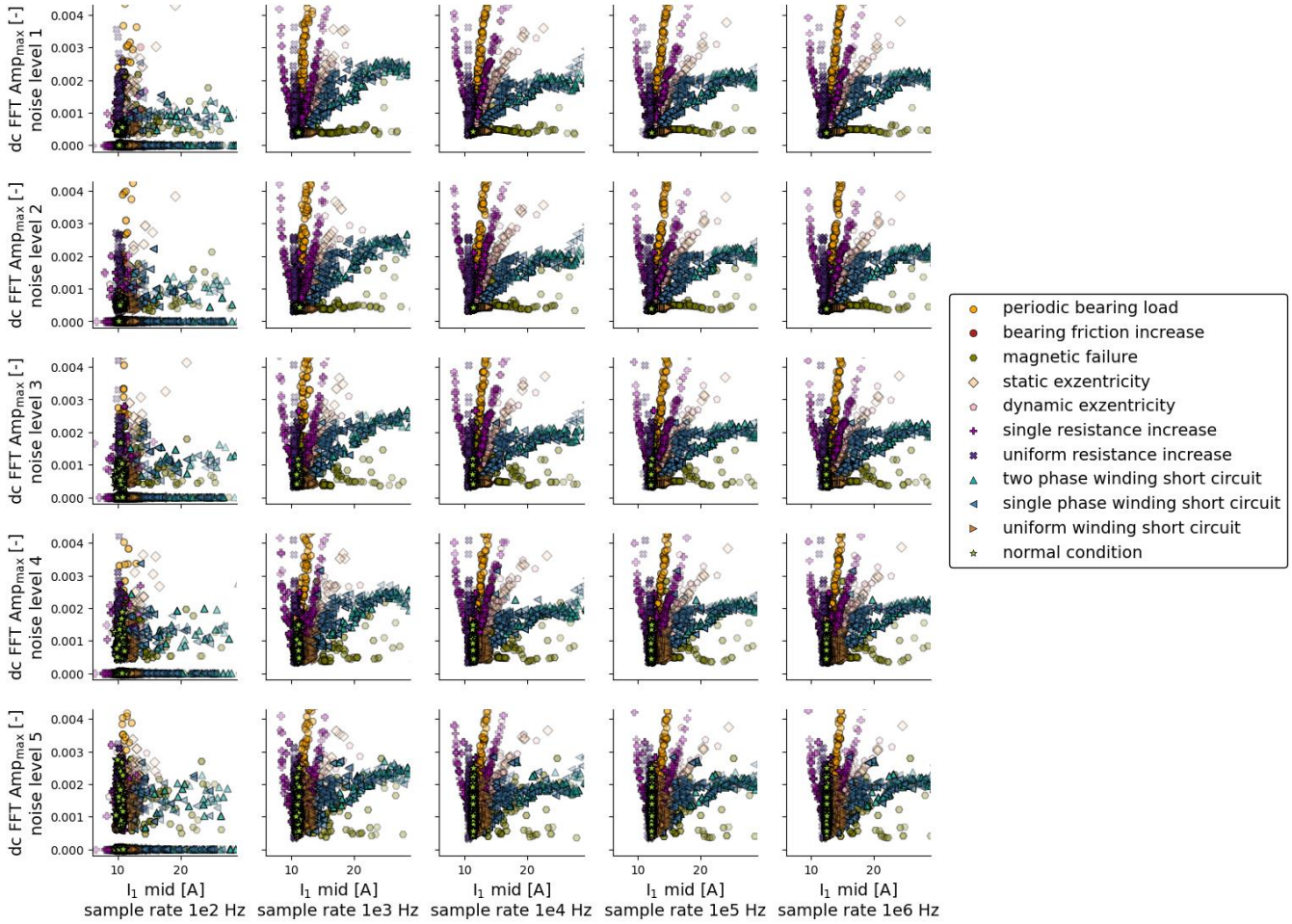

Figure 4. Influence of the sample rate and simulation noise on the generated features.

In figure 4 the intuitive assumption is confirmed that with increasing sample rate and decreasing noise individual classes become more distinguishable. With higher sample rate, there are more distinct directions away from the normal class, in which the features move with increasing degradation progress. Especially for the two lowest sample rates, it becomes apparent, that the frequency of the electric motor position passages cannot be resolved by them, resulting in less expressive features in the frequency domain. With increasing noise, the variance orthogonal to the trend with increasing degradation seems to increase as well. However the influence of the sample rate seems to be higher compared to the one of the noise, which can be due to the chosen ranges of noise and sample rate as well.

Table 3. Variance of class means for first two principal components.

	sample rate 1e2 Hz	**sample rate 1e3 Hz**	**sample rate 1e4 Hz**	**sample rate 1e5 Hz**	**sample rate 1e6 Hz**
noise level 1	0.370	0.389	0.399	0.480	0.477
noise level 2	0.379	0.405	0.416	0.491	0.479
noise level 3	0.429	0.450	0.459	0.522	0.480
noise level 4	0.379	0.409	0.416	0.475	0.442
noise level 5	0.343	0.357	0.364	0.433	0.433

The visible effect of sample rate and noise is also confirmed by the variance values in table 3 and 4. For high sample rate and low noise levels, the variance of the mean class values reaches its highest values, indicating a better distinguishability of the classes. On the other hand, the mean variance within classes decreases for high sample rates and low noise levels, indicating a closer arrangement within the classes. Interestingly the best values according to that interpretation can be found at a medium noise level and the second highest sample rate. This might indicate, that most of the relevant information can already be derived at those

signal levels. At the same time, however, the simple nature of this evaluation metric should not be overlooked, as higher variance might for example be quite desirable along axis indicating the degradation progress.

Table 4. Mean of class variances for first two principal components

	sample rate 1e2 Hz	sample rate 1e3 Hz	sample rate 1e4 Hz	sample rate 1e5 Hz	sample rate 1e6 Hz
noise level 1	0.695	0.673	0.661	0.566	0.562
noise level 2	0.680	0.650	0.637	0.550	0.560
noise level 3	0.606	0.583	0.573	0.504	0.551
noise level 4	0.676	0.639	0.631	0.565	0.599
noise level 5	0.725	0.712	0.704	0.620	0.610

A comparison of the voltage and temperature noise influence is given in figure 5, comparing the same selected features as in figure 2 and 4 and only taking into account the extrema of both noise levels, who are depicted for the medium sample rate. It becomes apparent, that especially the winding short circuit faults, marked with triangles in the figure, are more sensitive towards voltage noise compared to temperature noise. As the voltage noise seems to be more influential on the variance of most of the classes compared to the temperature noise, adjustments to their scale might be interesting in further simulations.

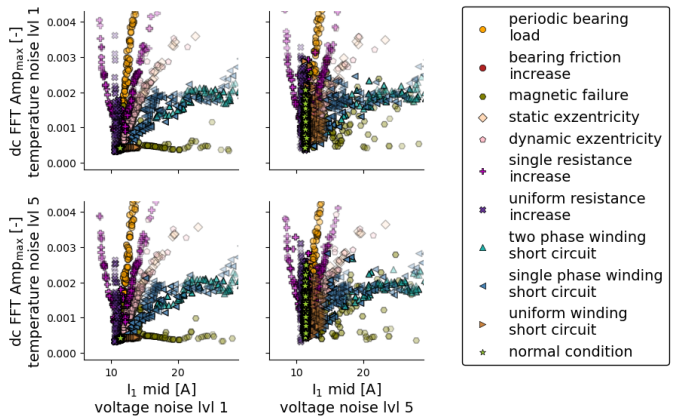

Figure 5. Influence of noise on the feature datasets.

4. Classification Capabilities

In table 5 the classification accuracies with optimized hyperparamters for the different algorithms depending on the sample rate are listed for the lowest noise level. They are trained on the full dataset and with encouraged feature reduction. In the results, the ensemble methods RF and XGB outperform the DT and SVM especially for smaller sample rates with the DT achieving results close to those of the ensemble methods for higher sample rates and the SVM being outperformed by the DT for higher sample rates. It is also visible, that the highest sample rate of 1e6 Hz does not bring further improvement compared to 1e5 Hz. The feature reduction slightly increased the performance of the DT and SVM here while slightly decreasing the performance of the ensemble methods. The obtained accuracies are considerably distant from one, due to a high influenced of the first degradation stage, which contains no previous degradation and just a tiny growth of it during the simulation, but might also be conditioned by the rather small dataset and shallow architecture of the algorithms.

Table 5. Classification accuracy on lowest noise level.

	DT	RF	XGB	SVM
sample rate 1e2 Hz	0.6887	0.7452	0.7369	0.6901
sample rate 1e3 Hz	0.8147	0.843	0.8423	0.801
sample rate 1e4 Hz	0.8678	0.8843	0.8705	0.8202
sample rate 1e5 Hz	0.8726	0.8898	0.8822	0.8506
sample rate 1e6 Hz	0.8726	0.8836	0.8898	0.823

The influence of the combined voltage and temperature noise on the classification is quantified at two different sample rates for each algorithm in table 6 considering all degradation progresses. It becomes apparent, that the noise especially influences the algorithm performance for small sample rates. For higher sample rates, it seems to effect the SVM and partially the DT but not influential on the ensemble methods anymore. A comparison of the influence of voltage and temperature noise shows, that the average performance decrease on the whole dataset is 3.33 % with fixed temperature and varied voltage noise and a less significant 0.158 % with varied temperature and fixed voltage noise.

Table 6. Classification accuracy depending on noise level.

	sample rate 1e3 Hz				sample rate 1e5 Hz			
	DT	RF	XGB	SVM	DT	RF	XGB	SVM
Noise level 1	0.8147	0.843	0.8423	0.801	0.8726	0.8898	0.8822	0.8506
Noise level 2	0.801	0.8182	0.8278	0.7603	0.8554	0.8767	0.874	0.7941
Noise level 3	0.7961	0.8175	0.8168	0.7176	0.8636	0.8891	0.8643	0.8003
Noise level 4	0.7872	0.8292	0.8209	0.7521	0.8588	0.876	0.8733	0.8629
Noise level 5	0.7652	0.8037	0.781	0.7686	0.8471	0.8747	0.8822	0.7713

The dependence of the classification performance on the analyzed degradation progress levels is quantified in table 7. It lists classification accuracies of the different algorithms for the highest sample rate and lowest noise for different subsets of the simulated datasets. Especially the first degradation stage raises problems for the algorithms. The subsets containing the first degradation stage perform noticeably worse than the others, even compared to a subset starting at the second degradation stage and omitting the last five. Without the first degradation stage, only the DT seems to profit from focusing on higher degradation levels, while the other algorithms perform fairly constant on the different subsets. Analogous to the noise influence depending on the sample rate, both influences do themselves depend on the analyzed degradation progresses and degrease with more distinguishable degradation progress.

Table 7. Classification accuracy depending on examined degradation stages.

	DT	RF	XGB	SVM
first to sixth degradation stage	0.8144	0.8270	0.8245	0.7967
all degradation stages	0.8726	0.8836	0.8898	0.8230
second to sixth degradation stage	0.9455	0.9697	0.9606	0.9742
all except first degradation stage	0.9447	0.9667	0.9591	0.9333
last 5 degradation stages	0.9758	0.9621	0.9561	0.9561

As all discussed results made use of feature reduction, in Table 8 the mean scores with and without feature reduction for the different algorithms are compared. This shows, that the feature reduction only has a small influence on the classification accuracy of the algorithms, slightly decreasing it for all except the DT. Paired with the reduction in complexity, the reduction of consulted features might still be attractive.

Table 8. Mean classification accuracy depending on feature selection method.

	DT	RF	XGB	SVM
all features	0.8343	0.8732	0.8634	0.8321
reduced features	0.8375	0.8636	0.8599	0.8243

The numbers of reduced features suggested by the hyperparameter optimization for the highest sample rate and lowest noise for the different degradation progress level sets are given in table 9. There is no clear indication of a dependency of the feature number and the complexity of the dataset. The RF does seem to work especially well with a small number of features while the XGB algorithm does require the highest amount of features under the analyzed conditions.

Table 9. Number of selected features depending on dataset.

	DT	RF	XGB	SVM
first to sixth degradation stage	18	8	14	13
all degradation stages	15	18	25	21
second to sixth degradation stage	20	8	21	22
all except first degradation stage	9	18	21	18
last 5 degradation stages	13	9	22	13

5. Regression Capabilities

As two different regression approaches are conducted, performing a regression on the whole dataset and on each classified class individually, those approaches are compared for the different algorithms in Table 10. For all regression tasks, the whole simulated dataset is used with all entries of the normal class having a degradation progress of Zero. Table 10 displays the regression results for the smallest noise level and varying sample rates. It is clearly visible, that the divided approach does lead to better results , unfortunately it did not converge for some SVM cases during a set training time limit, which is why their results were not included in the comparison. This may be due to the rather small datasets, when they are divided into single classes. For the approach on all classes, the SVMs perform poorer than the tree based methods as well with the DT coming closer to the ensemble methods in the all classes approach compared to the divided classes approach. The XGB produces the best results with the RF being in close range. The influence of the sample rate is visible for the lowest two sample rates, whose results are below those for the other sample rates, which all seem to be on a similar level.

Table 10. Root mean square regression error depending on sample rate.

	all classes				divided classes		
	DT	RF	XGB	SVM	DT	RF	XGB
sample rate 1e2 Hz	0.1970	0.1792	0.1745	0.3004	0.1192	0.1027	0.1039
sample rate 1e3 Hz	0.1661	0.1456	0.1577	0.1745	0.0885	0.0722	0.0781
sample rate 1e4 Hz	0.1428	0.1519	0.1268	0.1663	0.0719	0.0637	0.0583
sample rate 1e5 Hz	0.1371	0.1320	0.1277	0.1754	0.0801	0.0598	0.0646
sample rate 1e6 Hz	0.1372	0.1372	0.1288	0.1683	0.0733	0.0628	0.0652

Table 11 displays the results for a medium sample rate of 1e4 Hz and varying noise levels. The results contain a rather small influence of noise, especially for the undivided approach. For divided classes, the influence of noise is more prominent, which may be due to the smaller amount of data within divided classes.

Table 11. Root mean square regression error depending on noise.

	all classes				divided classes		
	DT	RF	XGB	SVM	DT	RF	XGB
Noise level 1	0.1428	0.1519	0.1269	0.1663	0.0719	0.0637	0.0583
Noise level 2	0.1458	0.1335	0.1358	0.1761	0.0757	0.0650	0.0619
Noise level 3	0.1532	0.1369	0.1461	0.1756	0.0807	0.0628	0.0679
Noise level 4	0.1520	0.1329	0.1389	0.2582	0.0769	0.0723	0.0725
Noise level 5	0.1464	0.1473	0.1414	0.1745	0.0877	0.0752	0.0725

6. Conclusion

By simulating the operation of a BLDC motor under varying conditions, the impact of noise, degradation process and sample rate on condition monitoring are investigated. It is shown, that lean algorithm architectures can produce satisfying results, with tree based methods being especially promising. Especially the ensemble methods RF and XGB show good robustness against decreasing data quality. Out of the analyzed influences, the sample rate turned out to be most influential on the performance. Resolving the electric motor position passages within the sample rate significantly improves the algorithms performance, with the results for lower sample rates still being useful indicators on the motor

condition. It also becomes clear, that lower data quality on one of the analyzed conditions increases the influence of the other ones on the results. Out of the degradation stages, the first one turns out to be hardly distinguishable for the various degradation mechanisms with the other ones having a much smaller effect on the classification results. For a regression on the degradation progress, dividing the fault classes by a preceding classification leads to considerably better results, which may be further improved with more datapoints within classes. Therefore, further simulations involving larger data sets with more degradation levels may be of interest for future research, as well as the inclusion of larger noise levels and varying loads.

ACKNOWLEDGEMENT

This project is funded by the funded by the Deutsche Forschungsgemeinschaft (DFG, German Research Foundation) under the project number 447676110, whose support is highly appreciated by the author. Furthermore, the author would like to thank Mr. Zhixiang Wang and Ms. Leonie Mathes for their contributions to the BLDC data analysis in the context of their master's theses.

REFERENCES

Akiba, T.; Sano, S.; Yanase, T.; Ohta, T.; Koyama, M. (2019): Optuna: A Next-generation Hyperparameter Optimization Framework.

AlShorman, O.; Irfan, M.; Saad, N.; Zhen, D.; Haider, N.; Glowacz, A.; AlShorman, A. (2020): A Review of Artificial Intelligence Methods for Condition Monitoring and Fault Diagnosis of Rolling Element Bearings for Induction Motor. In Shock and Vibration 2020, pp. 1–20. DOI: 10.1155/2020/8843759.

Bertolino, A. C.; Martin, A. d.; Jacazio, G.; Sorli, M. (2023): Design and Preliminary Performance Assessment of a PHM System for Electromechanical Flight Control Actuators. In Aerospace 10 (4), p. 335. DOI: 10.3390/aerospace10040335.

Chen, T.; Guestrin, C. (2016): XGBoost: A Scalable Tree Boosting System. DOI: 10.48550/arXiv.1603.02754.

Gupta, A.; Jayaraman, K.; Reddy, R. S. (2021): Performance Analysis and Fault Modelling of High Resistance Contact in Brushless DC Motor Drive. In : IECON 2021 - 47th Annual Conference of the IEEE Industrial Electronics Society. Toronto, ON, Canada, 13.10.2021 - 16.10.2021: IEEE, pp. 1–6.

Hasan, R.; Chu, C. (2022): Noise in Datasets: What Are the Impacts on Classification Performance? In : Proceedings of the 11th International Conference on Pattern Recognition Applications and Methods. SCITEPRESS - Science and Technology Publications, pp. 163–170.

Jiang, Z.; Han, Q.; Xu, X. (2020): Fault Diagnosis of Planetary Gearbox Based on Motor Current Signal Analysis. In Shock and Vibration 2020, pp. 1–13. DOI: 10.1155/2020/8854776.

Kudelina, K.; Asad, B.; Vaimann, T.; Rassolkin, A.; Kallaste, A.; Lukichev, D.V. (2020): Main Faults and Diagnostic Possibilities of BLDC Motors. In : 2020 27th International Workshop on Electric Drives: MPEI Department of Electric Drives 90th Anniversary (IWED). Moscow, Russia, 27.01.2020 - 30.01.2020: IEEE, pp. 1–6.

Lei, Y.; He, Z.; Zi, Y.; Hu, Q. (2007): Fault diagnosis of rotating machinery based on multiple ANFIS combination with GAs. In Mechanical Systems and Signal Processing 21 (5), pp. 2280–2294. DOI: 10.1016/j.ymssp.2006.11.003.

Nectoux, P.; Gouriveau, R.; Medjaher, K.; Ramasso, E.; Chebel-Morello, B.; Zerhouni, N.; Varnier, C. (2012): PRONOSTIA: An experimental platform for bearings accelerated degradation tests. In Proceedings of the IEEE International Conference on Prognostics and Health Management. hal-00719503

Pedregosa, F.; Varoquaux, G.; Gramfort, A.; Michel, V.; Thirion, B.; Grisel, O. et al. (2012): Scikit-learn: Machine Learning in Python. DOI: 10.48550/arXiv.1201.0490.

Shifat, T. A.; Hur, J. W. (2020): An Effective Stator Fault Diagnosis Framework of BLDC Motor Based on Vibration and Current Signals. In IEEE Access 8, pp. 106968–106981. DOI: 10.1109/ACCESS.2020.3000856.

Siddiolo, A. M.; Buderath, M. (2018): Development of a Prognostic Framework. In 10th International Symposium on NDT in Aerospace. Available online at https://www.ndt.net/?id=23873.

Weigert, M. (2022): Approach to Condition Monitoring of BLDC Motors with Experimentally Validated Simulation Data. In PHME_CONF 7 (1), pp. 521–529. DOI: 10.36001/phme.2022.v7i1.3357.

Wolfram, D.; Vogel, F.; Stauder, D. (2018): Condition monitoring for flight performance estimation of small multirotor unmanned aerial vehicles. In : 2018 IEEE Aerospace Conference. Big Sky, MT, 03.03.2018 - 10.03.2018: IEEE, pp. 1–17.

BIOGRAPHIES

Max Weigert received a M.Sc. in Mechanical and Process Engineering from Technische Universität Darmstadt in 2020. Afterwards, he became a research associate at the Institute of Flight Systems and Automatic Control at Technische Universität Darmstadt. Funded by the German Research Foundation, his research aims at a dynamic data-based estimation of the technical mission risk of unmanned aerial systems.